GPS Solutions (2019) 23:62
https://doi.org/10.1007/s10291-019-0845-z

ORIGINAL ARTICLE

Fuzzy-adaptive constrained data fusion algorithm for indirect centralized integrated SINS/GNSS navigation system

Sadra Rafatnia[1] · Hossein Nourmohammadi[2] · Jafar Keighobadi[1]

Received: 8 November 2018 / Accepted: 11 March 2019

Abstract
The main challenge of low-cost strap-down inertial navigation systems (SINSs) is time-growing positioning error due to erroneous measurements of micro-electro mechanical system (MEMS)-based inertial sensors. The global navigation satellite system (GNSS) provides drift-free positioning data that can be appropriately utilized to prevent the cumulative error of stand-alone SINS. The primary aim of this research is to enhance the positioning accuracy, performance, and reliability of low-cost SINS/GNSS-integrated navigation system. To attain this, we propose an applied data fusion algorithm for indirect centralized (IC) integrated SINS/GNSS. The proposed data fusion algorithm is based on fuzzy-adaptive constrained estimation filter. Velocity and altitude constraints are embedded in the integration scheme of the proposed SINS/GNSS system to preserve system reliability during abrupt GNSS outage. In an innovative way, the state constraints of altitude are defined based on the measurements of air-data sensors. The state estimation is effectively optimized since the respective states are projected on a constraint surface. Furthermore, a fuzzy type-2 inference system is developed for adaptively changing the covariance matrix of the estimation algorithm. Inertial measurements are used as the input of the fuzzy inference system. Accordingly, the state estimation algorithm is adaptively modified based on the vehicle's maneuvering during the navigation trajectory. The proposed SINS/GNSS system is experimentally assessed through several vehicular tests. The results indicate that not only does the proposed algorithm improve the navigation accuracy, it will also enhance the reliability of the integrated navigation system during GNSS outage.

Keywords SINS/GNSS · Data fusion · Fuzzy type-2 · Low-cost navigation · MEMS-grade IMU

Introduction

Advances in micro-electro mechanical system (MEMS)-based inertial sensors have brought about revolutionary progresses in low-cost strap-down inertial navigation systems (SINSs). In the SINS, inertial measurements of three-axis accelerometer and gyroscope are processed in a navigation computation unit and consequently, the navigation parameters including orientation, position, and velocity components are determined in a predefined coordinate system. During the navigation computation, the measurement errors of the accelerometers and gyroscopes are propagated over time as a quadratic and cubic error, respectively. This time-growing navigation error is the main drawback of the stand-alone SINS.

The global navigation satellite system (GNSS) has some complementary characteristics that can be appropriately integrated with SINS to develop an integrated SINS/GNSS system (Nourmohammadi and Keighobadi 2018a). On the other hand, GNSS signal may be obstructed because of underpasses, tall trees and buildings. In fact, a GNSS-denied environment leads to some undesirable effects. For example, inherent instability in the vertical channel of the SINS causes divergence in the altitude and vertical velocity estimation (Rafatnia et al. 2018). These effects should be kept to a minimum level to maintain the accurate values of vehicle position and velocity in GNSS-denied environments. Therefore, owing to covering the deficiencies of each stand-alone SINS and GNSS, the integrated SINS/GNSS system provides more accurate and reliable navigation data. However, the integration mechanization plays a substantial role in the performance of the SINS/GNSS navigation system. This becomes more crucial as low-cost inertial measurement units (IMUs) are used in the SINS.

✉ Hossein Nourmohammadi
hnourmhammadi@tabrizu.ac.ir;
hnourmohammadi@yahoo.com

[1] Department of Mechanical Engineering, University of Tabriz, Tabriz, Iran

[2] Malek Ashtar University of Technology, Tehran, Iran

Published online: 11 April 2019

Kalman filter (KF) is one of the efficient approaches to integrate the SINS with the GNSS. In this methodology, the SINS states are estimated based on the position and velocity measurements of the GNSS. Regarding SINS/GNSS systems, several KF-based integration algorithms can be found in the literature, such as extended Kalman filter (EKF) (Faruqi and Turner 2000), sigma-point Kalman filter (SPKF) (van der Merwe et al. 2004), quadratic Kalman filter (QKF) (Wang et al. 2006), unscented Kalman filter (UKF) (Hu et al. 2015), robust Kalman filter (RKF) (Zhao et al. 2016), cubature Kalman filter (CKF) (Zhao 2016), augmented CKF (Wang et al. 2017), and QR-factorized CKF (Nourmohammadi and Keighobadi 2017). In some research, artificial intelligence-based algorithms have been developed to enhance the performance of SINS/GNSS systems. For example, Musavi and Keighobadi (2015) used fuzzy neural network approach to approximate the IMU uncertainties in the SINS/GNSS system. El-Shafie et al. (2014) developed wavelet-ANFIS-based integration scheme for vehicular navigation applications. Yao et al. (2017) proposed a hybrid data fusion algorithm based on neural network and KF for application in the integrated SINS/GNSS system. Rafatnia et al. (2018) developed a recurrent wavelet neural network (RWNN)-based algorithm for the integration of low-cost SINS with global positioning system (GPS).

Nourmohammadi and Keighobadi (2018b) presented a new classification for loosely coupled SINS/GNSS systems based on indirect centralized (IC) and direct decentralized (DD) integration schemes. Here, we concentrate on IC integrated SINS/GNSS in which the SINS error dynamics are used in the centralized filter of the state estimation algorithm. We develop fuzzy adaptive constrained data fusion algorithm to enhance the navigation accuracy and reliability of the IC integrated SINS/GNSS system. In the presented algorithm, the normalized output of the inertial sensors is analyzed as the input of the proposed fuzzy type-2 inference system. Accordingly, the designed data fusion scheme is automatically tuned and the system noise covariance matrix is adaptively adjusted based on the vehicle's maneuver during the navigation trajectory. Furthermore, in the proposed integration scheme, two applied altitude and velocity constraints are defined and a constrained state estimation filter is constituted. After calibration of air-data sensors including barometer and thermometer with respect to different environmental conditions in the form of standard and non-standard atmosphere models, the true barometric altitude is calculated and accordingly, the vehicle altitude constraints are defined. The altitude constraints in combination to vehicle velocity constraints are used to project the respective states on a constraint surface. As a main superiority in comparison with the classical unconstrained filters, the proposed constrained filter is able to achieve a great performance of integrated SINS/GNSS system during GNSS outage. The main contributions can be summarized as follows:

- Design of fuzzy-adaptive integration scheme for SINS/GNSS navigation system in which the system noise covariance matrix is automatically adjusted based on the maneuvering level in the navigation trajectory.
- Dynamically calculation of true altitude constraints based on calibrated air-data system for application in integrated inertial navigation algorithms.
- Design of constrained data fusion algorithm for SINS/GNSS system based on altitude and velocity constraints to enhance the system reliability during GNSS outage.

Strap-down inertial navigation mechanization

Strap-down inertial navigation technology is a major mechanical simplification of the traditional stable-platform navigation system. In the strap-down mechanization, the inertial sensors are rigidly attached on the body of the host (under-navigation) vehicle. The linear acceleration and angular rate of the host vehicle are measured in body frame by the embedded three-axis accelerometer and gyroscope. These measurements are mathematically processed in the computation unit of the strap-down INS. Accordingly, the navigation parameters including orientation angles, position, and velocity components are determined in a predefined coordinate frame. The following sections describe the main mechanization of the SINS comprising SINS dynamics and SINS error dynamics.

SINS dynamics

As shown in Fig. 1, the main coordinate frames of the SINS are earth-centered earth-fixed (ECEF) frame, inertial frame, body frame, and navigation frame which are specified by subscripts "*e*", "*i*", "*b*", and "*n*", respectively. The e-frame has origin at the earth center and rotates in the inertial space to remain fixed with respect to the earth surface. The b-frame is directly defined on the body center of the host vehicle. The n-frame is constituted by north–east–down coordinates as a local-level navigation frame.

The SINS position dynamics including latitude (L), longitude (l), and altitude (h) are described as follows (Titterton and Weston 2018):

$$\dot{L} = \frac{v_{\mathrm{N}}}{R_{\mathrm{N}} + h} \quad , \quad \dot{l} = \frac{v_{\mathrm{E}}}{(R_{\mathrm{E}} + h)\cos L} \quad , \quad \dot{h} = -v_{\mathrm{D}} \tag{1}$$

where R_{N} and R_{E} stand for meridian and transverse radii of curvature, respectively. The north, east, and down velocity components in the n-frame are updated based on the following dynamics (Titterton and Weston 2018):

$$\dot{v}_{\mathrm{N}} = f_{\mathrm{N}} - v_{\mathrm{E}}\left(2\omega_{\mathrm{e}} + \frac{v_{\mathrm{E}}}{(R_{\mathrm{E}} + h)\cos L}\right)\sin L + \frac{v_{\mathrm{D}} v_{\mathrm{N}}}{R_{\mathrm{N}} + h} \tag{2}$$

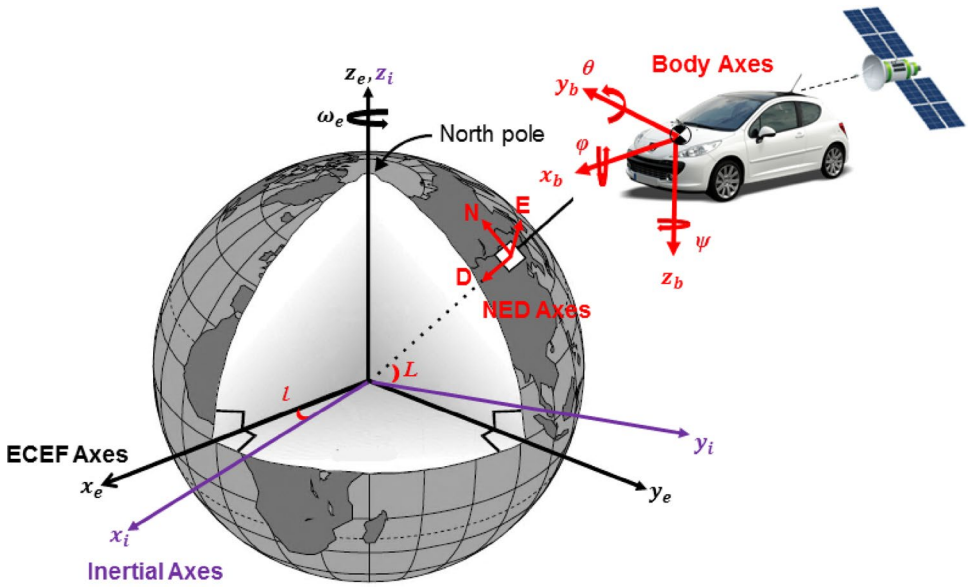

Fig. 1 Reference coordinate frames in inertial navigation

$$\dot{v}_{\mathrm{E}} = f_{\mathrm{E}} - 2\omega_{\mathrm{e}}\left(v_{\mathrm{N}}\sin L + v_{\mathrm{D}}\cos L\right) + \frac{v_{\mathrm{E}}}{R_{\mathrm{E}}+h}\left(v_{\mathrm{D}} + v_{\mathrm{N}}\sin L\right) \tag{3}$$

$$\dot{v}_{\mathrm{D}} = f_{\mathrm{D}} - v_{\mathrm{E}}\left(2\omega_{\mathrm{e}} + \frac{v_{\mathrm{E}}}{(R_{\mathrm{E}}+h)\cos L}\right)\cos L - \frac{v_{\mathrm{N}}^2}{R_{\mathrm{N}}+h} + g \tag{4}$$

where, ω_{e} is the earth rate and g is gravitational acceleration. $\boldsymbol{f}^{\mathrm{n}} = \left[f_{\mathrm{N}}\ f_{\mathrm{E}}\ f_{\mathrm{D}}\right]^{\mathrm{T}}$ is the specific force vector in the n-frame. $\boldsymbol{f}^{\mathrm{n}}$ is calculated from the accelerometer output vector in the b-frame, $\boldsymbol{f}^{\mathrm{b}}$, in accordance with the following vector transformation:

$$\boldsymbol{f}^{\mathrm{n}} = \left[f_{\mathrm{N}}\ f_{\mathrm{E}}\ f_{\mathrm{D}}\right]^{\mathrm{T}} = \boldsymbol{C}_{\mathrm{b}}^{\mathrm{n}}\boldsymbol{f}^{\mathrm{b}} \tag{5}$$

where $\boldsymbol{C}_{\mathrm{b}}^{\mathrm{n}}$ stands for the rotation/transformation matrix from the b-frame to the n-frame. Considering *Z–Y–X* sequence for the Euler angles, $\boldsymbol{C}_{\mathrm{b}}^{\mathrm{n}}$ is defined as (Milanchian et al. 2015)

$$\mathbf{C}_{\mathrm{b}}^{\mathrm{n}} = \begin{bmatrix} C\theta\,C\psi & -C\varphi\,S\psi + S\varphi\,S\theta\,C\psi & S\varphi\,S\psi + C\varphi\,S\theta\,C\psi \\ C\theta\,S\psi & C\varphi\,C\psi + S\varphi\,S\theta\,S\psi & -S\varphi\,C\psi + C\varphi\,S\theta\,S\psi \\ -S\theta & S\varphi\,C\theta & C\varphi\,C\theta \end{bmatrix} \tag{6}$$

As shown in Fig. 1, the angles φ, θ, and ψ are roll (bank), pitch (elevation) and yaw (heading), respectively. In (6), the symbols C and S stand for cosine and sine functions, respectively. The time-derivative of the rotation matrix, $\boldsymbol{C}_b^n$, is given by Titterton and Weston (2018):

$$\dot{\mathbf{C}}_b^n = \mathbf{C}_b^n\,\boldsymbol{\Omega}_{nb}^b \tag{7}$$

where $\boldsymbol{\Omega}_{\mathrm{nb}}^{\mathrm{b}}$ is a skew-symmetric matrix with elements from vector $\boldsymbol{\omega}_{\mathrm{nb}}^{\mathrm{b}}$ representing the rotation rate of the b-frame relative to the n-frame.

SINS error dynamics

The SINS error state vector is constituted by misalignment error ($\delta\alpha,\ \delta\beta,\ \delta\gamma$), velocity error ($\delta v_{\mathrm{N}},\ \delta v_{\mathrm{E}},\ \delta v_{\mathrm{D}}$), position error ($\delta L,\ \delta l,\ \delta h$), gyroscope drifts ($D_{\mathrm{N}},\ D_{\mathrm{E}},\ D_{\mathrm{D}}$) and accelerometer bias ($B_{\mathrm{N}},\ B_{\mathrm{E}},\ B_{\mathrm{D}}$); note that the accelerometer bias and gyroscope drift have been defined in the n-frame. The linearized form of the SINS error dynamics in the n-frame is expressed as follows (Nourmohammadi and Keighobadi 2018c):

$$\begin{aligned}
\delta\dot{\alpha} &= -\left(\omega_{\mathrm{e}}\sin L + \frac{v_{\mathrm{E}}}{R_{\mathrm{E}}+h}\tan L\right)\delta\beta + \frac{v_{\mathrm{N}}}{R_{\mathrm{N}}+h}\delta\gamma + \frac{1}{R_{\mathrm{E}}+h}\delta v_{\mathrm{E}} - \omega_{\mathrm{e}}\sin L\delta L - \frac{v_{\mathrm{E}}}{\left(R_{\mathrm{E}}+h\right)^2}\delta h - D_{\mathrm{N}} \\
\delta\dot{\beta} &= \left(\omega_{\mathrm{e}}\sin L + \frac{v_{\mathrm{E}}}{R_{\mathrm{E}}+h}\tan L\right)\delta\alpha + \left(\omega_{\mathrm{e}}\cos L + \frac{v_{\mathrm{E}}}{R_{\mathrm{E}}+h}\right)\delta\gamma - \frac{1}{R_{\mathrm{N}}+h}\delta v_{\mathrm{N}} + \frac{v_{\mathrm{E}}}{\left(R_{\mathrm{N}}+h\right)^2}\delta h - D_{\mathrm{E}} \\
\delta\dot{\gamma} &= -\frac{v_{\mathrm{N}}}{R_{\mathrm{N}}+h}\delta\alpha - \left(\omega_{\mathrm{e}}\cos L + \frac{v_{\mathrm{E}}}{R_{\mathrm{E}}+h}\right)\delta\beta - \frac{\tan L}{R_{\mathrm{E}}+h}\delta v_{\mathrm{E}} - \left(\omega_{\mathrm{e}}\cos L + \frac{v_{\mathrm{E}}}{\left(R_{\mathrm{E}}+h\right)\cos^2 L}\right)\delta L \\
&\quad + \frac{v_{\mathrm{E}}\tan L}{\left(R_{\mathrm{E}}+h\right)^2}\delta h - D_D
\end{aligned} \tag{8}$$

$$
\begin{aligned}
\delta\dot{v}_{\mathrm{N}} &= -f_{\mathrm{D}}\delta\beta + f_{\mathrm{E}}\delta\gamma + \frac{v_{\mathrm{D}}}{R_{\mathrm{N}}+h}\delta v_{\mathrm{N}} - 2\sin L\left(\omega_{\mathrm{e}} + \frac{v_{\mathrm{E}}}{(R_{\mathrm{E}}+h)\cos L}\right)\delta v_{E} + \frac{v_{\mathrm{N}}}{R_{\mathrm{N}}+h}\delta v_{\mathrm{D}} \\
&\quad - \left(2\omega_{\mathrm{e}} v_{\mathrm{E}}\cos L + \frac{v_{\mathrm{E}}^2}{(R_{\mathrm{E}}+h)\cos^2 L}\right)\delta L + \left(\frac{v_{\mathrm{E}}^2\tan L}{(R_{\mathrm{E}}+h)^2} - \frac{v_{\mathrm{N}}v_{\mathrm{D}}}{(R_{\mathrm{N}}+h)^2}\right)\delta h + B_{\mathrm{N}} \\
\delta\dot{v}_{\mathrm{E}} &= f_{\mathrm{D}}\delta\alpha - f_{\mathrm{N}}\delta\gamma + \left(2\omega_{\mathrm{e}}\sin L + \frac{v_{\mathrm{E}}\tan L}{R_{\mathrm{E}}+h}\right)\delta v_{\mathrm{N}} + \left(\frac{v_{\mathrm{D}} + v_{\mathrm{N}}\tan L}{R_{\mathrm{E}}+h}\right)\delta v_{\mathrm{E}} \\
&\quad + \left(2\omega_{\mathrm{e}}\cos L + \frac{v_{\mathrm{E}}}{R_{\mathrm{E}}+h}\right)\delta v_{D} + \left(2\omega_{\mathrm{e}}\left(v_{\mathrm{N}}\cos L - v_{\mathrm{D}}\sin L\right) + \frac{v_{\mathrm{N}}v_{\mathrm{E}}}{(R_{\mathrm{E}}+h)\cos^2 L}\right)\delta L \\
&\quad - \left(\frac{v_{\mathrm{E}}\left(v_{\mathrm{D}} + v_{\mathrm{N}}\tan L\right)}{(R_{\mathrm{E}}+h)^2}\right)\delta h + B_{\mathrm{E}} \\
\delta\dot{v}_{\mathrm{D}} &= -f_{\mathrm{E}}\delta\alpha + f_{\mathrm{N}}\delta\beta - \frac{2v_{\mathrm{N}}}{R_{\mathrm{N}}+h}\delta v_{\mathrm{N}} - 2\left(\omega_{\mathrm{e}}\cos L + \frac{v_{\mathrm{E}}}{R_{\mathrm{E}}+h}\right)\delta v_{\mathrm{E}} + 2\omega_{\mathrm{e}} v_{\mathrm{E}}\sin L\delta L \\
&\quad + \left(\frac{v_{\mathrm{E}}^2}{(R_{\mathrm{E}}+h)^2} + \frac{v_{\mathrm{N}}^2}{(R_{\mathrm{N}}+h)^2} - \frac{2g}{R+h}\right)\delta h + B_{\mathrm{D}}
\end{aligned}
\tag{9}
$$

$$
\begin{aligned}
\delta\dot{L} &= -\frac{v_{\mathrm{N}}}{(R_{\mathrm{N}}+h)^2}\delta h + \frac{1}{R_{\mathrm{N}}+h}\delta v_{\mathrm{N}} \\
\delta\dot{l} &= \frac{v_{\mathrm{E}}\sin L}{(R_{\mathrm{E}}+h)\cos^2 L}\delta L - \frac{v_{\mathrm{E}}}{(R_{\mathrm{E}}+h)^2\cos L}\delta h + \frac{1}{(R_{\mathrm{E}}+h)\cos L}\delta v_{\mathrm{E}} \\
\delta\dot{h} &= -\delta v_{\mathrm{D}}
\end{aligned}
\tag{10}
$$

$$
\begin{aligned}
\dot{D}_i &= -\beta D_i + \sigma\sqrt{2\beta}w(t) \qquad i = N, E, D \\
\dot{B}_i &= -\beta B_i + \sigma\sqrt{2\beta}w(t) \qquad i = N, E, D
\end{aligned}
\tag{11}
$$

Note that, the accelerometer bias and gyroscope drift have been formulated based on first-order Gauss–Markov model. In (11). σ and β are variance and correlation coefficient of the Gauss–Markov process, respectively. According to (8)–(11), the state vector of the SINS error model is constructed as follows:

$$
\boldsymbol{x} = \left[\,\delta\alpha\ \ \delta\beta\ \ \delta\gamma\ \ \delta v_{\mathrm{N}}\ \ \delta v_{\mathrm{E}}\ \ \delta v_{\mathrm{D}}\ \ \delta L\ \ \delta l\ \ \delta h\ \ D_{\mathrm{N}}\ \ D_{\mathrm{E}}\ \ D_{\mathrm{D}}\ \ B_{N}\ \ B_{\mathrm{E}}\ \ B_{\mathrm{D}}\,\right]^{\mathrm{T}} \tag{12}
$$

Using (8) through (11), the estimated position and velocity components are corrected as follows:

$$
\begin{aligned}
L &= \hat{L} - \delta L \\
l &= \hat{l} - \delta l \\
h &= \hat{h} - \delta h
\end{aligned}
\tag{13}
$$

$$
\begin{aligned}
v_{\mathrm{N}} &= \hat{v}_{\mathrm{N}} - \delta v_{\mathrm{N}} \\
v_{\mathrm{E}} &= \hat{v}_{\mathrm{E}} - \delta v_{\mathrm{E}} \\
v_{\mathrm{D}} &= \hat{v}_{\mathrm{D}} - \delta v_{\mathrm{D}}
\end{aligned}
\tag{14}
$$

where the symbol (^) denotes the estimated quantity and that without (^) is the corrected quantity. In addition, the rotation matrix is corrected by use of the misalignment matrix based on the following equation:

$$
\hat{\boldsymbol{C}}_{\mathrm{b}}^{\mathrm{n}} = [\boldsymbol{I} - \boldsymbol{\Psi}]\boldsymbol{C}_{\mathrm{b}}^{\mathrm{n}} \tag{15}
$$

in which $\boldsymbol{\Psi}$ is a skew-symmetric matrix containing elements from the misalignment vector $\left[\,\delta\alpha\ \ \delta\beta\ \ \delta\gamma\,\right]^{\mathrm{T}}$,

$$
\boldsymbol{\Psi} = \begin{bmatrix} 0 & -\delta\gamma & \delta\beta \\ \delta\gamma & 0 & -\delta\alpha \\ -\delta\beta & \delta\alpha & 0 \end{bmatrix} \tag{16}
$$

Equation (15) is only valid for small misalignment angles. By incorporating (16) into (15), the estimated orientation angles of the SINS are also corrected.

Velocity and altitude constraints

In the low-cost SINS, the cumulative errors of inertial sensors lead to time-growing positioning error. This is the main drawback of the stand-alone SINS. Here, two applied constraints are proposed to limit the time-growing navigation error of the stand-alone SINS. As shown in Fig. 2, these auxiliary constraints include velocity constraints and altitude constraint. The velocity constraints are based on the assumption that the vertical and lateral velocity components in the b-frame are close to zero ($v_y = v_z = 0$). In addition, the longitudinal component is limited as follows:

$$
0 \le |v_x| \le v_{\max} \tag{17}
$$

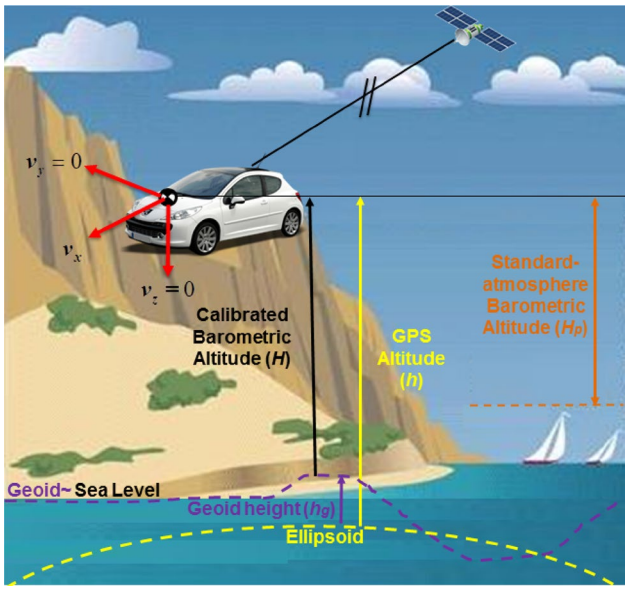

Fig. 2 Auxiliary altitude and velocity constrains for inertial navigation

in which v_{max} is the maximum admissible velocity of the host vehicle. The velocity constraints can be transformed from the b-frame to the n-frame as follows:

$$\begin{aligned} 0 \le |v_N| &\le |v_{max}(\cos\theta\cos\psi)| \\ 0 \le |v_E| &\le |v_{max}(\cos\theta\sin\psi)| \\ 0 \le |v_D| &\le |-v_{max}\sin\theta| \end{aligned} \tag{18}$$

Note that velocity constraints are especially applicable to the planar motion of the wheeled platform without lateral slippage. Barometric altitude is an appropriate measurement that can be used to enhance the accuracy of the SINS. However, it is different from the GNSS altitude. The barometric altitude is computed with respect to sea level. But, the GNSS altitude is the altitude above the reference ellipsoid that approximates the earth surface. Here, an applied algorithm is presented to develop altitude constraint from calibrated air-data sensors. In this respect, the barometric altitude is first computed for a non-standard atmosphere and then the SINS altitude constraint is constituted based on the calibrated barometric altitude. In the standard atmosphere, the temperature, T_0, and pressure, P_0, in sea level are assumed to be constant as 101.325 (kPa) and 288.15 (°K), respectively. However, in a real atmosphere, the temperature and pressure of sea level are often modeled by different air-data conditions. Hence, non-standard atmosphere strategy should be applied to enhance the air-data system performance.

In the standard atmosphere model, the barometric altitude, H_p, is given by (Rafatnia et al. 2018)

$$H_p = \frac{T_0}{L_a}\left[\left(\frac{P_s}{P_0}\right)^{-\frac{LR}{g}} - 1\right] + H_0 \tag{19}$$

where L_a and R are the constant lapse rate and universal gas constant, respectively. However, for non-standard atmosphere conditions, bias, b, and scale factor, s, are applied to calculate the calibrated altitude as follows:

$$H = H_P + s\,(H_P - H_0) + b \tag{20}$$

where the bias and scale factor are calculated as

$$\begin{aligned} s &= \frac{\Delta T}{T_0} \\ b &= \frac{RT_0}{g}\left(\frac{\Delta P}{P_0}\right) \end{aligned} \tag{21}$$

in which the deviation of true magnitude in the sea level from the standard condition in the case of temperature, $\Delta T = T_t - T_0$, and pressure, $\Delta P = P_t - P_0$, can be calculated using the following model (Rafatnia et al. 2018):

$$\begin{aligned} T_t &= T_s + L_a H_P \\ P_t &= P_s + \rho g H_p \end{aligned} \tag{22}$$

where T_t and P_t are the true temperature and pressure in the sea level, respectively, and the thermometer and barometer measurements are presented by T_s and P_s, respectively. Finally, by calculating the calibrated barometric altitude and with this assumption that the sea level is an approximation of geoid level, the SINS altitude constraint is constructed as follows:

$$\begin{aligned} &\text{if} \quad h_g > 0 \quad \text{then} \quad H < h < H + h_g \\ &\text{if} \quad h_g < 0 \quad \text{then} \quad H + h_g < h < H \end{aligned} \tag{23}$$

where h_g is the geoid height at the vehicle location based on the EGM96 earth model (Lemoine et al. 1997).

SINS/GNSS integration mechanization

The complementary characteristics of the GNSS and the SINS motivate the development of an integrated SINS/GNSS navigation system. Different algorithms have been proposed for SINS/GNSS navigation system. We concentrate on IC integrated SINS/GNSS in which the SINS error dynamics are used in the estimation process

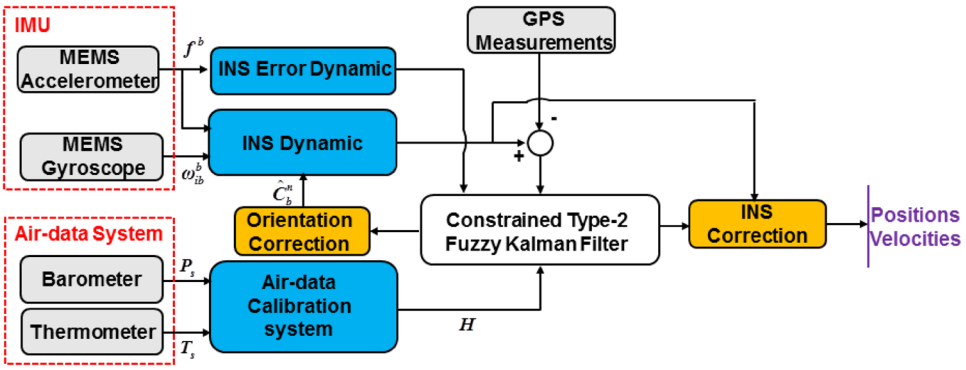

Fig. 3 Main mechanization of the proposed integrated SINS/GNSS system

(Nourmohammadi and Keighobadi 2018b). Here, a new data fusion algorithm is developed for IC integrated SINS/GNSS system. The major aim of the current research is to enhance the overall accuracy and reliability of the low-cost integrated inertial navigation systems. The block diagram of Fig. 3 shows the main configuration of the proposed integrated navigation system. Input data, dynamical systems, data fusion algorithm and measurement data are the main parts illustrated in the figure. Input data are supplied by inertial sensors including three-axis accelerometer and gyroscope, and also air-data sensors including barometer and thermometer. The dynamical systems in the proposed SINS/GNSS are divided into INS dynamics and INS error dynamics. The INS dynamics are constituted by the position, velocity, and orientation dynamics as expressed in (1), (2)–(4), and (7), respectively. The linearized form of the INS error dynamics has been described in (8)–(11). Data fusion process is exerted on the INS error dynamics. In fact, the navigation parameters, including orientation, position, and velocity, are not directly estimated. The INS error states are estimated in the data fusion process. Subsequently, the estimated error states are applied to correct the INS dynamics output. The measurement vector of the estimation algorithm is constituted by the INS dynamics output, GNSS data, and in some situations, barometric altitude. The data fusion algorithm of the proposed SINS/GNSS system is based on constrained type-2 fuzzy Kalman filter (T2FKF) approach. The performance of the proposed estimation filter is not conditioned by the stochastic noise covariance of the MEMS-grade inertial sensors. This is one of the main superiority aspects of the proposed approach in comparison with the conventional KF method. Furthermore, in the proposed constrained T2FKF, the velocity constraints of (18) and the altitude constraint of (23) are appropriately embedded in the integration scheme to maintain the navigation accuracy and reliability, especially during GNSS outages.

In summary, the proposed constrained T2FKF is implemented in four steps comprising time-update, measurement-update, covariance matrix matching, and state projection. In the following sections, the constrained T2FKF is described in detail.

Time update

In this step, the predicted values of error covariance, $\boldsymbol{P}_k^-$, and state vector, $\boldsymbol{x}_k^-$, are calculated as follows (Simon 2006):

$$\boldsymbol{P}_k^- = \boldsymbol{\Gamma}_{k-1}\boldsymbol{P}_{k-1}\boldsymbol{\Gamma}_{k-1}^{\mathrm{T}} + \boldsymbol{Q}_{k-1} \tag{24}$$

$$\hat{\boldsymbol{x}}_k^- = \boldsymbol{\Gamma}_{k-1}\hat{\boldsymbol{x}}_{k-1}^- \tag{25}$$

in which $\boldsymbol{\Gamma}_{k-1}$ is the state-transition matrix associating with the dynamic of the INS error model (8)–(11). $\boldsymbol{Q}_{k-1}$ stands for the covariance matrix of the system noise. It is updated during the covariance matrix matching process.

Measurements update

In this step, the Kalman gain, $\boldsymbol{K}_{\mathrm{k}}$, is calculated and consequently, the state vector and the error covariance matrix are updated as follows (Simon 2006):

$$\boldsymbol{K}_k = \boldsymbol{P}_k^-\boldsymbol{\Omega}_k^{\mathrm{T}}\left(\boldsymbol{\Omega}_k\boldsymbol{P}_k^-\boldsymbol{\Omega}_k^{\mathrm{T}} + \boldsymbol{R}_k\right)^{-1} \tag{26}$$

$$\hat{\boldsymbol{x}}_k = \hat{\boldsymbol{x}}_k^- + \boldsymbol{K}_k\left[z_k - \boldsymbol{\Omega}_k\hat{\boldsymbol{x}}_k^-\right] \tag{27}$$

$$\boldsymbol{P}_k = \left(\boldsymbol{I} - \boldsymbol{K}_k\boldsymbol{\Omega}_k\right)\boldsymbol{P}_k^- \tag{28}$$

where $\boldsymbol{R}_{\mathrm{k}}$ is the covariance matrix of the measurement noise. $\boldsymbol{\Omega}_{\mathrm{k}}$ characterizes the observation matrix which is constructed based on the state vector, $\hat{\boldsymbol{x}}_{\mathrm{k}}$, and the measurement vector, z_{k}, as follows:

$$\boldsymbol{\Omega}_{\mathrm{k}} = \begin{bmatrix} 0_{3\times3} & \boldsymbol{I}_{3\times3} & 0_{3\times3} & 0_{3\times3} & 0_{3\times3} \\ 0_{3\times3} & 0_{3\times3} & \boldsymbol{I}_{3\times3} & 0_{3\times3} & 0_{3\times3} \end{bmatrix} \tag{29}$$

$$z_{\mathrm{k}} = \left[\, \boldsymbol{v}^{\mathrm{INS}} - \boldsymbol{v}^{\mathrm{GPS}} \;\; \boldsymbol{r}^{\mathrm{INS}} - \boldsymbol{r}^{\mathrm{GPS}} \,\right]^{\mathrm{T}} \tag{30}$$

in which $\boldsymbol{v} = \left[v_N \; v_E \; v_D \right]^T$ and $\boldsymbol{r} = \left[L \; l \; h \right]^T$ are the velocity and the position vectors, respectively. Also, the superscript INS characterizes the output of the INS dynamics expressed in (1)–(4).

Covariance matrix update

According to (24), the performance of the Kalman filter estimation algorithm is significantly related to the covariance matrix of the system noise. The measurement reliability in MEMS-grade IMUs is related to vehicle maneuvering (Nourmohammadi and Keighobadi 2018c). Therefore, in the error covariance prediction, a proper covariance matrix is required in accordance with the system noise. In this study, an adaptive covariance matching algorithm is proposed based on a type-2 fuzzy logic. In the proposed algorithm, the maneuvering level of the vehicle is evaluated through the IMU measurements. Accordingly, the following parameters are defined as input to the type-2 fuzzy inference system.

$$\xi_1 = \left\| f^b \right\|_2 = \sqrt{\sum_{i=x,y} \left(f_i^b \right)^2 + \left(f_z^b + g \right)^2} \tag{31}$$

$$\xi_2 = \left\| \boldsymbol{\omega}_{nb}^b \right\|_1 = \sum_{i=x,y,z} \left| \boldsymbol{\omega}_i^b \right| \tag{32}$$

A normalizing factor, α, is defined as the output of fuzzy inference system. α is used to update the covariance matrix based on the following relationship:

$$Q_k = Q_0 \times 10^{\alpha} \tag{33}$$

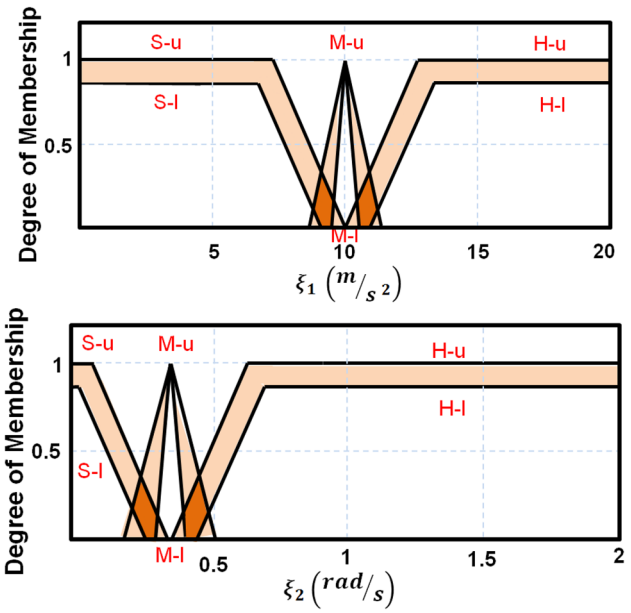

Fig. 4 Membership functions of input variables

Expert knowledge is applied to characterize the fuzzy system input ξ_1 and ξ_2. Three linguistic type-2 fuzzy sets including small (S), medium (M), and high (H) are considered for the input variables ξ_1 and ξ_2. Figure 4 shows the membership functions of the fuzzy sets, S, M, and H, corresponding to each input.

The membership functions of Fig. 4 have been designed based on the experience and the knowledge of expert engineers in the field of inertial navigation. Accordingly, the following linguistic fuzzy rule-base, comprising of nine rules, is developed:

$$\begin{aligned}
&\text{if } \xi_1 \text{ is Small and } \xi_2 \text{ is Small then } \alpha = -1\\
&\text{if } \xi_1 \text{ is Small and } \xi_2 \text{ is Medium then } \alpha = -0.5\\
&\text{if } \xi_1 \text{ is Medium and } \xi_2 \text{ is Small then } \alpha = -0.25\\
&\text{if } \xi_1 \text{ is Medium and } \xi_2 \text{ is Small then } \alpha = -0.75\\
&\text{if } \xi_1 \text{ is Medium and } \xi_2 \text{ is Medium then } \alpha = 0\\
&\text{if } \xi_1 \text{ is Medium and } \xi_2 \text{ is High then } \alpha = 0.25\\
&\text{if } \xi_1 \text{ is High and } \xi_2 \text{ is Small then } \alpha = 0.5\\
&\text{if } \xi_1 \text{ is High and } \xi_2 \text{ is Medium then } \alpha = 0.75\\
&\text{if } \xi_1 \text{ is High and } \xi_2 \text{ is High then } \alpha = 1
\end{aligned} \tag{34}$$

Therefore, α is adaptively determined in the proposed fuzzy inference system based on the maneuvering level of the host vehicle along with the navigation trajectory. Then, the covariance matrix, Q_k, is adjusted based on (33).

Estimation projection

In the constrained T2FKF estimation algorithm, the following minimization problem is executed in the presence of the INS error model constraints (Simon 2010):

$$\tilde{x}_k = \arg\min_{x_k} \left(x_k - \hat{x}_k \right)^T W \left(x_k - \hat{x}_k \right) \tag{35}$$

Subject to: $Dx_k \leq d_k$

where $\tilde{x}$ stands for the projected state on the constraints surface. W is a positive-definite weighting matrix. D and d are known matrices representing the standard form of the constraints:

$$D = \begin{bmatrix}
0_{2\times3} & \begin{bmatrix} 1 \\ -1 \end{bmatrix} & 0_{2\times1} & 0_{2\times1} & 0_{2\times2} & 0_{2\times1} & 0_{2\times6} \\
0_{2\times3} & 0_{2\times1} & \begin{bmatrix} 1 \\ -1 \end{bmatrix} & 0_{2\times1} & 0_{2\times2} & 0_{2\times1} & 0_{2\times6} \\
0_{2\times3} & 0_{2\times1} & 0_{2\times1} & \begin{bmatrix} 1 \\ -1 \end{bmatrix} & 0_{2\times2} & 0_{2\times1} & 0_{2\times6} \\
0_{2\times3} & 0_{2\times1} & 0_{2\times1} & 0_{2\times1} & 0_{2\times2} & \begin{bmatrix} 1 \\ -1 \end{bmatrix} & 0_{2\times6}
\end{bmatrix} \tag{36}$$

$$d_k = \begin{bmatrix} v_N - v_{\max}(\cos\theta\cos\psi) \\ v_N \\ v_E - v_{\max}(\cos\theta\sin\psi) \\ v_E \\ v_D + v_{\max}\sin\theta \\ v_D \\ h - H - h_g \\ -h + H \end{bmatrix}$$

The problem (35) with the inequality constraints of (36) could be solved by use of the active set method (Fletcher 2013). In this method, the active constraints in the solution are determined first, and then the problem solution is stated as follows:

$$\bar{x}_k = \tilde{x}_k - W^{-1}\hat{D}^T\left(\hat{D}W^{-1}\hat{D}^T\right)^{-1}\left(\hat{D}\tilde{x} - \hat{d}_k\right) \quad (37)$$

where $\hat{D}$ and $\hat{d}_k$ are the row of D and the components of d_k that are active at the problem solution.

Experimental results and discussion

For implementation of the proposed constrained T2FKF on the IC integrated SINS/GNSS navigation system, some vehicular field tests have been carried out by experienced colleagues in University of Tabriz. The test equipment is shown in Fig. 5. The ADIS-16407 IMU has been used to provide linear acceleration and angular rate. Moreover, the barometer and thermometer are also combined to supply the air-data measurements. The reference position and velocity data of the vehicle are presented by a Garmin-35 GPS receiver with 1 Hz updating rate. The main statistical specifications of the inertial sensors in ADIS-16407 IMU are given in Table 1.

Table 1 Main specifications of inertial sensors in ADIS-16,407

Parameters	Gyroscope	Accelerometer
Misalignment (axis-to-frame)	0.05°	0.2°
Misalignment (axis-to-axis)	0.5°	0.5°
Initial bias error (1σ)	3°/s	50 mg
In-run bias stability (1σ)	0.007°/s	0.2 mg
Random walk (1σ)	$1.9°/\sqrt{\text{h}}$	$0.2\ \text{m/s}/\sqrt{\text{h}}$
Output noise (no filtering)	0.8 deg/s rms	9 mg rms

To verify the proposed constrained T2FKF integration algorithm, two vehicular tests with various dynamical maneuvering have been designed. Figure 6 presents the reference latitude–longitude and altitude trajectories of the vehicle in test #1. As shown in the figure, test #1 has been executed in 500 s, approximately. According to the top panel, the vehicle started to move from point P_1 and continues up to P_7 with several circular maneuvers. In addition, some GPS outage environments with different strategies considered as short time (P_2–P_3), long time (P_4–P_5) and stationary (P_6) navigation. The intervals of GNSS outage have been created artificially through the off-line analysis. The GNSS data existing in reality during these intervals were used as a reference.

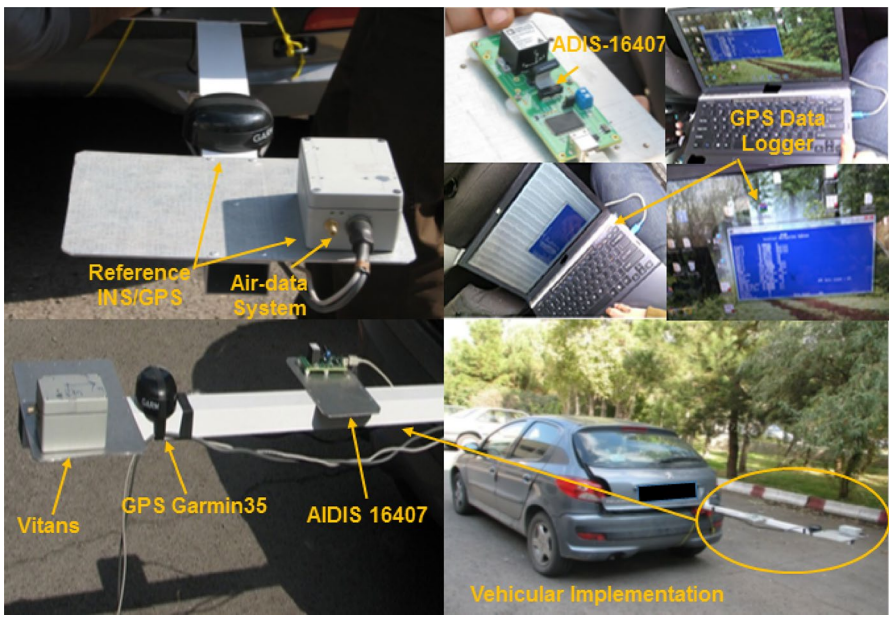

Fig. 5 Vehicular navigation test

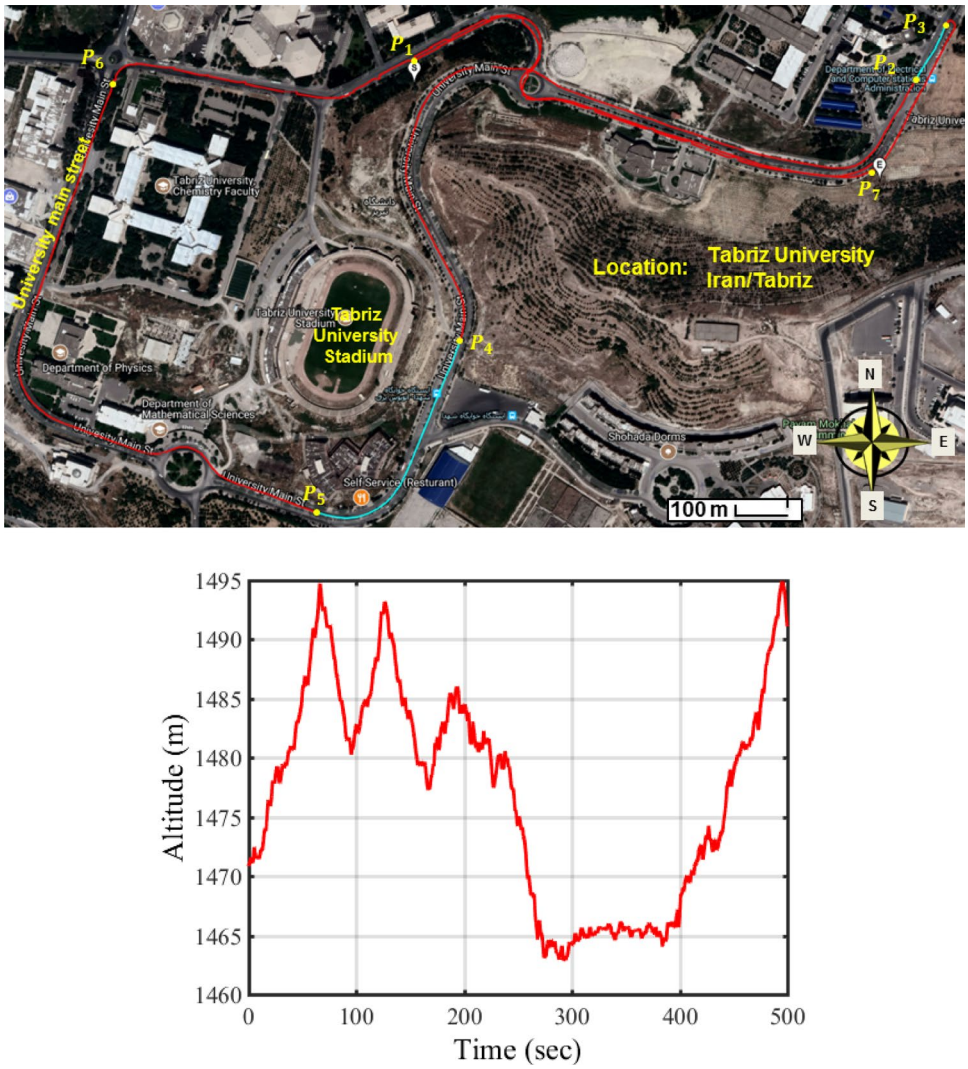

Fig. 6 Test #1. Reference latitude–longitude trajectory (top), reference altitude trajectory (bottom)

In this section, two different strategies of T2FKF are employed for IC integrated SINS/GNSS. In the first strategy, called "Cons.T2FKF", the estimation filter is focused on the constraints of velocity and altitude during GPS outage. In the second strategy, called "Uncons.T2FKF", the state constraints are dropped.

The estimated latitude–longitude trajectory of the vehicle for both "Cons.T2FKF" and "Uncons.T2FKF"-based integrated navigation algorithms in test #1 is shown in Fig. 7. For better evaluation, the estimation error of the position and the velocity components with respect to the reference GPS data are shown in Figs. 8 and 9, respectively. It is clearly seen that the performance of both "Cons.T2FKF" and "Uncons.T2FKF" are nearly close to the reference GPS data while GPS data are available. However, during GPS outage a considerable estimation error can be seen in the case of "Uncons.T2FKF" estimation algorithm. Especially, in the stationary point, P_6, "Cons.T2FKF" has better estimation accuracy in comparison with "Uncons.T2FKF". Moreover, the altitude error is increased in the case of "Uncons. T2FKF". The inefficiency of "Uncons.T2FKF" is mainly due to vertical channel instability in the strap-down INS. On the other hand, "Cons.T2FKF" algorithm successfully satisfies the state constraints and prevents incremental estimation error especially in altitude estimation.

For a better comparison of "Cons.T2FKF" and "Uncons. T2FKF", the mean value and the standard deviation of the estimation error are reported in Table 2. The statistical results of Table 2 indicate that the proposed constrained T2FKF-based SINS/GNSS yields to superior position and velocity estimation in comparison with the unconstrained T2FKF-based one. However, the differences between these

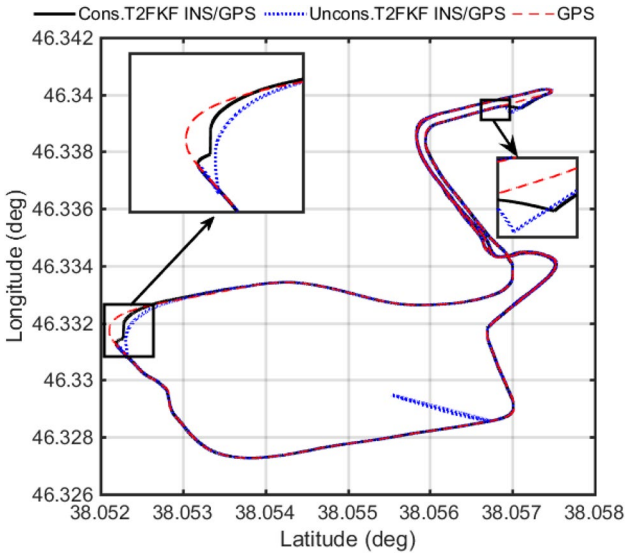

Fig. 7 Estimated trajectories through both "Cons.T2FKF" and "Uncons.T2FKF" in SINS/GNSS compared to the reference GPS data in test #1

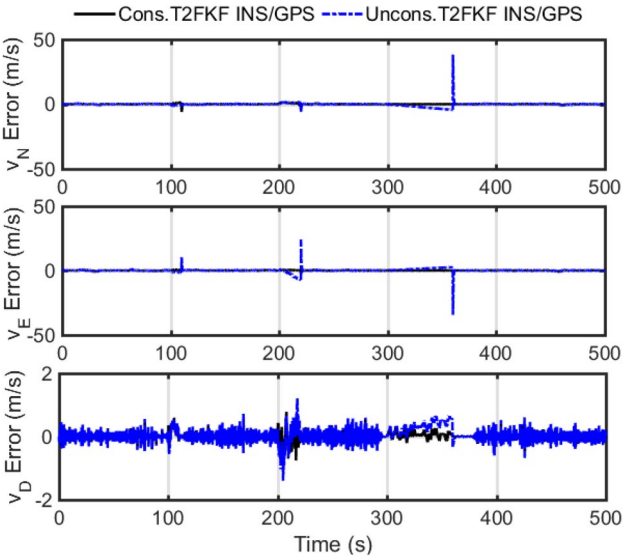

Fig. 9 Estimated errors of the velocity components through both "Cons.T2FKF" and "Uncons.T2FKF" in test #1

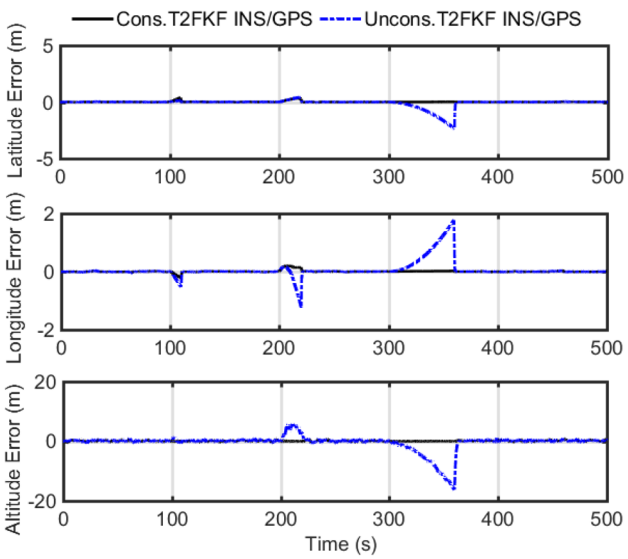

Fig. 8 Estimated errors of the position components through both "Cons.T2FKF" and "Uncons.T2FKF" in test #1

strategies are highlighted in the performance of navigation system during GPS outage. For example, the mean value and the standard deviation of estimation error of altitude in the "Cons.T2FKF" algorithm are much less than in "Uncons. T2FKF". This is because of focusing on velocity and altitude constraints in harsh environments.

To legitimize the performance, reliability and accuracy assessment of the proposed constrained T2FKF algorithm, the proposed data fusion method is compared with conventional Kalman filter method in another vehicular test. Test #2 with different maneuvers and considered GPS outage has been designed at the University of Tabriz. This test takes 400 s, approximately. Figure 10 represents the reference geographical latitude–longitude trajectory and reference altitude trajectory in test #2. As shown in Fig. 10 (bottom), the vehicle experienced higher altitude maneuvering in test #2 compared to test #1. In test #2, the vehicle starts its motion in P_1 and continues up to P_8. The GPS signal blockage is occurred in distance between P_2–P_3, P_4–P_5, and P_6–P_7.

Figure 11 shows the latitude–longitude trajectory obtained by both "Cons.T2FKF" and "Uncons.KF" (unconstrained Kalman filter)-based SINS/GNSS during test#2. The performance of "Cons.T2FKF" method in view of the navigation accuracy and reliability during GPS outage and the satisfaction of the SINS state constraints are better than for "Uncons.KF". In addition, as shown in Figs. 12 and 13, the estimation error of the position and the velocity components through the proposed ''Cons.T2FKF'' is lower than for "Uncons.KF". According to Fig. 12, "Uncons.KF"-based SINS/GNSS has undesirable responses regarding the estimation of altitude during signal blockage of GPS.

To have a comprehensive comparison between different strategies in the cases of "Uncons.KF" and "Cons.T2FKF" integration algorithms, the mean value and the standard

Table 2 Mean value and standard deviation of the estimation error in test #1

Navigation parameter	IC integrated SINS/GNSS with constrained T2FKF integration		IC integrated SINS/GNSS with unconstrained T2FKF integration	
	Mean value of estimation error	Standard deviation of estimation error ($\pm 1\sigma$)	Mean value of estimation error	Standard deviation of estimation error ($\pm 1\sigma$)
Latitude error (m)	0.0122	0.0531	− 0.217	0.72
Longitude error (m)	0.007	0.0374	0.154	0.55
Altitude error (m)	0.108	0.2362	− 1.38	5.112
V-north error (m/s)	0.0435	0.301	− 0.3844	1.954
V-east error (m/s)	0.0059	0.2	0.1121	0.22
V-down error (m/s)	0.011	0.1279	0.065	0.223

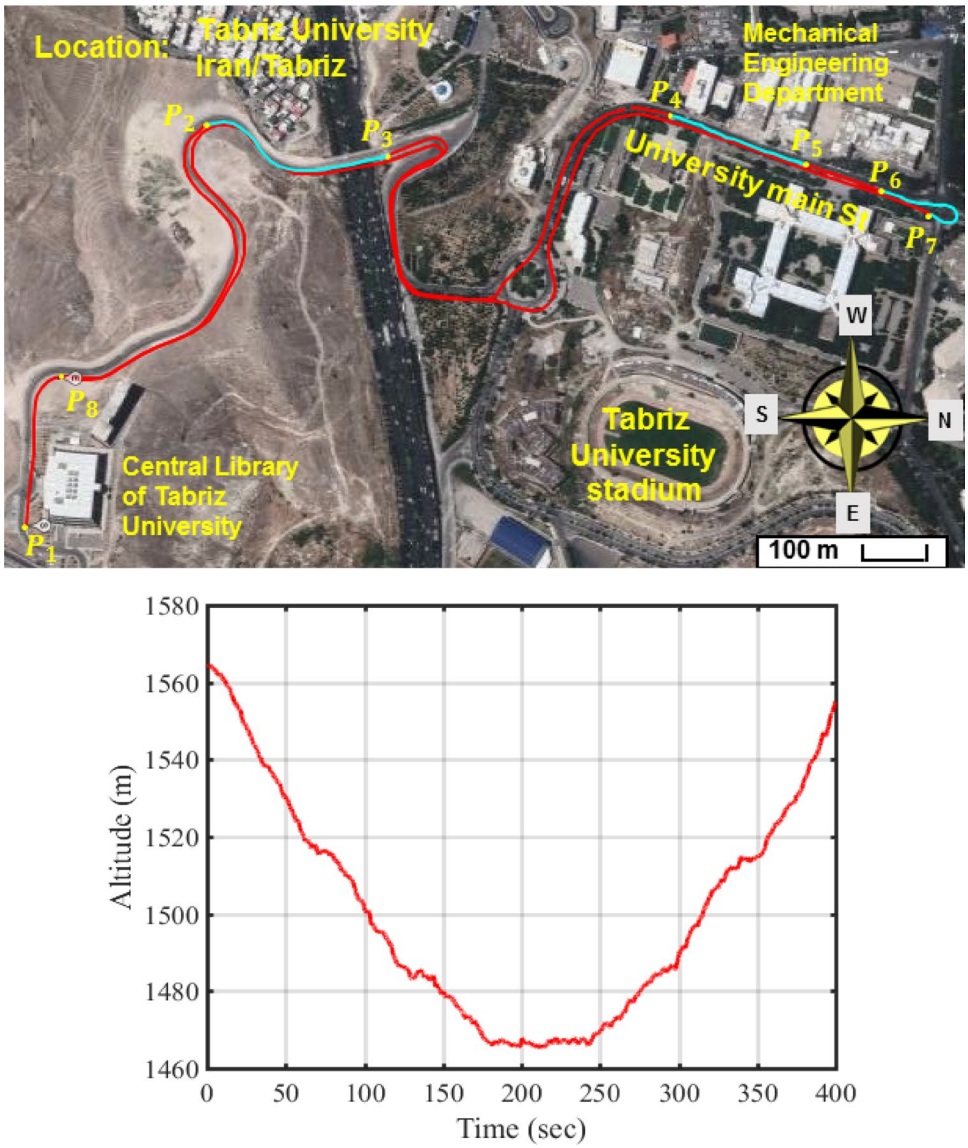

Fig. 10 Test #2 reference latitude–longitude trajectory (top) and reference altitude trajectory (bottom)

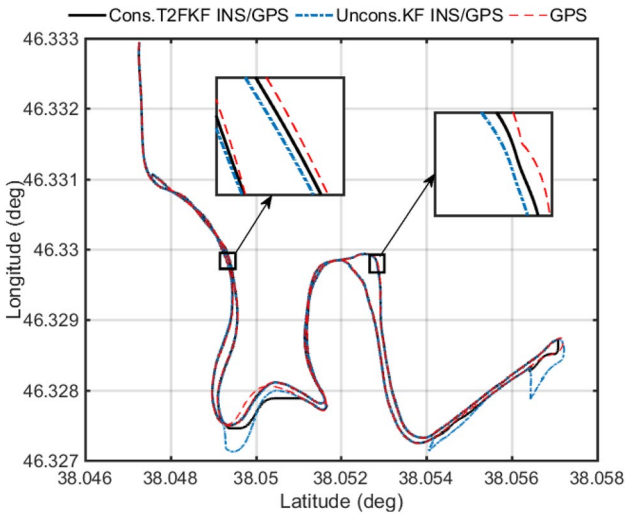

Fig. 11 Estimated trajectories through both "Cons.T2FKF" and "Uncons.KF" in SINS/GNSS compared to the reference GPS data in test #2

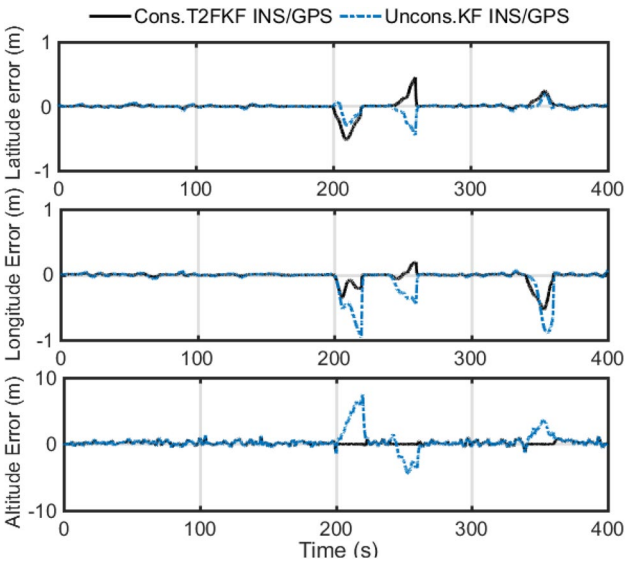

Fig. 12 Estimated errors of the position components through both "Cons.T2FKF" and "Uncons.KF" in test #2

deviation of the estimation errors in test #2 are reported in Table 3.

The statistical results of Table 3 indicate that the proposed type-2 fuzzy logics can assist the navigation accuracy via adaptively changing of the covariance matrix of the system noise. However, the differences between these strategies

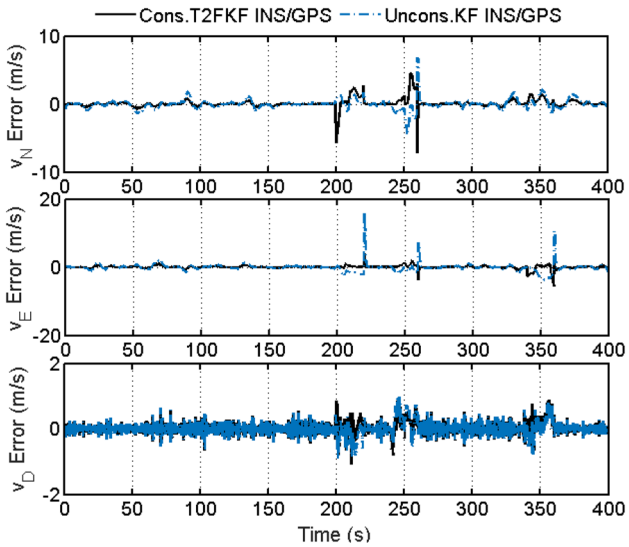

Fig. 13 Estimated errors of the velocity components through both "Cons.T2FKF" and "Uncons.KF" in test#2

are highlighted in the performance and the reliability during GPS outage.

Conclusions

Motivated by enhancing the navigation reliability and accuracy of the low-cost SINS/GNSS system, an adaptive constrained integration algorithm has been presented in this research work. In the proposed approach, the constraints of the stand-alone SINS are defined based on the combination of calibrated air-data sensors output and some auxiliary constraints in velocity components. Type-2 fuzzy logics are defined to determine adaptively the covariance matrix of the system noise in various driving conditions. Accordingly, the integrated system is tuned online for different vehicle maneuvering. The proposed integration scheme has been verified with different vehicular tests under various dynamical maneuvering. The results indicated that the proposed adaptive constrained approach leads to the improved navigation accuracy. Moreover, the constraints of stand-alone SINS enhanced the reliability of integrated system during GNSS outage. It has been revealed that the proposed "Cons.T2FKF"-based SINS/GNSS causes higher navigation accuracy and reliability in comparison with "Uncons.T2FKF" and "Uncons.KF"-based algorithms.

Table 3 Mean value and standard deviation of the estimation error in test #2

Navigation parameter	IC integrated SINS/GNSS with constrained T2FKF integration		IC integrated SINS/GNSS with unconstrained KF integration	
	Mean value of estimation error	Standard deviation of estimation error ($\pm 1-$)	Mean value of estimation error	Standard deviation of estimation error ($\pm 1-$)
Latitude error (m)	– 0.002	0.049	– 0.014	0.067
Longitude error (m)	– 0.023	0.088	– 0.063	0.183
Altitude error (m)	0.15	0.281	0.75	1.285
V-north error (m/s)	0.013	0.501	– 0.017	0.743
V-east error (m/s)	– 0.008	0.66	– 0.171	1.12
V-down error (m/s)	0.006	0.157	0.008	0.183

References

El-Shafie A, Najah A, Karim OA (2014) Amplified wavelet-ANFIS-based model for GPS/INS integration to enhance vehicular navigation system. Neural Comput Appl 24(8):1905–1916

Faruqi FA, Turner KJ (2000) Extended Kalman filter synthesis for integrated global positioning/inertial navigation systems. Appl Math Comput 115(2):213–227

Fletcher R (2013) Practical methods of optimization. Wiley, Hoboken

Hu G, Gao S, Zhong Y (2015) A derivative UKF for tightly coupled INS/GPS integrated navigation. ISA transactions 56:135–144

Lemoine FG et al (1997) The development of the NASA GSFC and NIMA joint geopotential model. The International Association of Geodesy Symposia, IAG Symposia, Berlin

Milanchian H, Keighobadi J, Nourmohammadi H (2015) Magnetic calibration of three-axis strapdown magnetometers for applications in MEMS attitude-heading reference systems. AUT J Model Simul 47(1):55–65

Musavi N, Keighobadi J (2015) Adaptive fuzzy neuro-observer applied to low-cost INS/GPS. Appl Soft Comput 29:82–94

Nourmohammadi H, Keighobadi J (2017) Decentralized INS/GNSS system with MEMS-grade inertial sensors using QR-factorized CKF. IEEE Sens J 17(11):3278–3287

Nourmohammadi H, Keighobadi J (2018a) Integration scheme for SINS/GPS system based on vertical channel decomposition and in-motion alignment. AUT J Model Simul 50(1):13–22

Nourmohammadi H, Keighobadi J (2018b) Design and experimental evaluation of indirect centralized and direct decentralized integration scheme for low-cost INS/GNSS system. GPS Solut 22(3):1–18

Nourmohammadi H, Keighobadi J (2018c) Fuzzy adaptive integration scheme for low-cost SINS/GPS navigation system. Mech Syst Signal Process 99:434–449

Rafatnia S, Nourmohammadi H, Keighobadi J, Badamchizadeh MA (2018) In-move aligned SINS/GNSS system using recurrent wavelet neural network (RWNN)-based integration scheme. Mechatronics 54:155–165

Simon D (2006) Optimal state estimation: Kalman, H infinity, and nonlinear approaches. Wiley, Hoboken

Simon D (2010) Kalman filtering with state constraints: a survey of linear and nonlinear algorithms. IET Control Theory Appl 4(8):1303–1318

Titterton S, Weston JL (2018) Strapdown inertial navigation technology. The Institution of Engineering and technology, IET, London

van der Merwe R, Wan E, Julier S (2004) Sigma-point Kalman filters for nonlinear estimation and sensor-fusion: applications to integrated navigation. In: AIAA guidance navigation, and control conference and exhibit, Providence, Rhode Island, 16–19 August 2004. https://doi.org/10.2514/6.2004-5120

Wang W, Liu ZY, Wie RR (2006) Quadratic extended Kalman filter approach for GPS/INS integration. Aerosp Sci Technol 10(8):709–713

Wang D, Lv H, Wu J (2017) Augmented cubature Kalman filter for nonlinear RTK/MIMU integrated navigation with non-adaptive noise. Measurement 97:111–125

Yao Y, Xu X, Zhu C, Chan CY (2017) A hybrid fusion algorithm for GPS/INS integration during GPS outages. Measurement 103:42–51

Zhao Y (2016) Performance evaluation of cubature Kalman filter in a GPS/IMU tightly coupled navigation system. Signal Process 119:67–79

Zhao L, Qiu H, Feng Y (2016) Analysis of a robust Kalman filter in loosely coupled GPS/INS navigation system. Measurement 80:138–147

Sadra Rafatnia received the B.Sc. degree in Mechanical Engineering from Guilan University, Rasht, Iran, in (2012) and the M.Sc. degree in Mechanical Engineering from Tabriz University, Tabriz, Iran, in (2015). He is currently a Ph.D. student in Mechanical Engineering at Sahand University of Technology (SUT). He has been a Research Assistant with the Dynamic, Vibration and Control laboratory at SUT since (2016). His current research interests include nonlinear control, estimation and optimization theory.

Hossein Nourmohammadi received the B.Sc. degree in Mechanical Engineering from Nooshirvani University of Technology, Babol, Iran, in 2010, the M.Sc. degree in Mechanical Engineering from Amirkabir University of Technology (Tehran Polytechnic), Tehran, Iran, in 2012 and Ph.D. degree in Mechanical Engineering at University of Tabriz, Iran, in 2017. He has been a Research Assistant with the Guidance, Navigation, and Control (GNC) laboratory at University of Tabriz since 2013. His current research interests include GNC, integrated navigation systems, estimation and identification, and nonlinear adaptive control.

Jafar Keighobadi received the B.Sc. degree in Mechanical Engineering from University of Tabriz, Tabriz, Iran, in 1997, and M.Sc. and Ph.D. degrees in Mechanical Engineering and Control Systems from Department of Mechanical Engineering, Amirkabir University of technology (Tehran Polytechnic), Tehran, Iran, in 2000 and 2008, respectively. He is currently an Associate Professor of Mechanical Engineering Department, University of Tabriz. His research interests include artificial intelligence, estimation and identification, nonlinear robust control, and GNC.